RSC Advances

ROYAL SOCIETY OF CHEMISTRY

www.rsc.org/advances

RSC Advances

RSCPublishing

PAPER

Easily deconstructed, high aspect ratio cellulose nanofibres from *Triodia pungens*; an abundant grass of Australia's arid zone

Nasim Amiralian[1], Pratheep K. Annamalai[1], Paul Memmott[2], Elena Taran[3], Susanne Schmidt[4], Darren J. Martin*[1]

Cite this: DOI: 10.1039/x0xx00000x
Received 00th January 20XX,

Accepted 00th January 20XX

DOI: 10.1039/x0xx00000x

www.rsc.org/

The production of high aspect ratio cellulose nanofibres without resorting to very harsh mechanical and/or chemical processing steps remains a challenge that hinders progress in the fast-moving nanocellulose field. In response to this challenge, herein we report the preparation of high aspect ratio (>500) and small diameter (<8 nm) cellulose nanofibrils through the deconstruction of Australian native 'spinifex' grass (*Triodia pungens*) by applying very mild pulping conditions combined with only one pass of high pressure homogenization. Spinifex grass has an unusually high hemicellulose content, which facilitates this easy fibrillation process. Tensile measurements of the nanopaper produced by vacuum filtration indicated a high toughness of about 12 MJm^{-3}, a tensile strength of 82 MPa and a high elongation at break of 18 %. The transverse elastic modulus of single nanofibrils analysed by AM-FM is in the range of 19 - 24 GPa. Under these mild processing conditions, *Triodia pungens* nanofibrils retained their crystallinity.

Introduction

Recently the deconstruction of primary cellulose fibres into nanoscale fibres has become a topic of intense fundamental and applied research. These nanofibres are well-known for their unique structure and many useful characteristics, with a large number of applications emerging in multiple industrial sectors. Cellulose nanofibres can be either highly crystalline, rigid rod-like nanocrystals (cellulose nanocrystals, CNC), or long, moderately crystalline filament-like nanofibrils (microfibrillated cellulose (MFC) and nanofibrillated cellulose (NFC)).[1] Cellulose nanocrystals (CNC) are routinely obtained via acid hydrolysis, ultra-sonication, mechanical and enzymatic treatments or combinations thereof,[1-4] while MFC and NFC are usually obtained using mechanical shearing or fibrillation methods.[5-9] The mechanical methods currently employed consume energy at different levels and result in different types of MFC and NFC, depending also on the cellulose raw material source.[5]

Nanofibrillated cellulose with a diameter below 20 nm and length of few micrometers[1] requires higher energy inputs for fibrillation and generally is produced through the use of mechanical methods such as homogenization, ultrasonication, milling, or a combination of these methods following chemical (e.g. TEMPO oxidation, carboxymethylation), mechanical or enzymatic pretreatments of the highly purified wood or plant fibres. In comparison, MFC with fibre diameters in the range of 20 - 100 nm are commonly produced via similar mechanical treatments from purified fibres, but without the application of additional biomass pretreatment.[10-13] An important consideration is that the application of intense mechanical energy causes fracture of cellulose fibres, thereby reducing their length and aspect ratio. To avoid this damage and loss of aspect ratio, cellulosic fibres can be treated by employing multiple, but more gentle mechanical processing treatments to facilitate the gradual breakdown of the fibre into more intact nanoscale fibrils. For example, cellulosic feedstock materials may be passed through high pressure or high shear homogenizers or disc refiners several times (up to 20, 30 or even 150 passes in some examples).[14, 15] In current commercial practice, this multi-step processing results in high energy costs and long processing times which reduces the commercial attractiveness of the product. This implies that the production of high-aspect ratio (longer and thinner) cellulose nanofibres using lower energy and chemical input remains one of the primary technological challenges.[16, 17] In this work we produced high aspect ratio NFC from bleached spinifex pulp without the need for further chemical, enzymatic, or mechanical pretreatments.[18]

Spinifex grasses form the dominant vegetation of Australia's semi-arid hummock grasslands that cover nearly one third of the continent (≈2.1 million km^2). Spinifex is the common name for species in the tribe Triodieae (genera *Triodia*, *Monodia*, and

Symplectrodia [19, 20]) of which the genus *Triodia* is the dominant genus with 69 identified species today. Endemic to Australia, spinifex grasses are perennial evergreen xerophytes adapted to dry and hot environments.[19, 21] They have highly resilient prickly leaves ,[22, 23] and based on anatomy and resin production, are classified into non-resinous "hard" species and resinous "soft" species.[19, 22, 24-26] *Triodia pungens* was studied here as one of the most abundant resinous species with an extensive distribution in the semi-arid regions north of 27 °S latitude across the continent.[27] In this study, the morphology, crystalline structure and mechanical properties of *T. pungens* nanofibrils were compared with some other sources of cellulose reported in the literature. Moreover, for meaningful benchmarking purposes, a commercially available pure form of cellulose i.e. 'microcrystalline cellulose (MCC)' was exposed to identical homogenization processing and compared to the spinifex-derived NFC.

Material and Methods

Materials

We collected mature *Triodia pungens* plants near Camooweal, north-west Queensland, Australia. Microcrystalline cellulose Avicel PH-101 NF (Farm grade) was purchased from FMC Biopolymers, Philadelphia, United States. The chemicals employed in this study included sodium hydroxide, glacial acetic acid (Ajax Finechem, Thermo Fischer Pty Ltd, Scoresby, Australia), sodium chlorite technical grade, 80% (Sigma-Aldrich, Castle Hill, Australia), and all reagents were used as-received.

Pulping method

After being washed with hot water and air dried, *T. pungens* was cut to an approximate fibre length of 0.3 - 7 mm and an average fibre diameter of 63 ± 38 µm, then delignified at 80 °C for two hours using a 2 % (w/v) sodium hydroxide solution with a 10:1 solvent to grass ratio, followed by rinsing the product with 60 °C water. The delignified fibres were then twice bleached using an acidic solution of 1 % (w/v) sodium chlorite at 70 °C for one hour with a 30:1 solvent to grass ratio (pH=4, the pH was decreased with glacial acetic acid). Based on the TAPPI standard, a compositional analysis was carried out on both washed and bleached pulped spinifex (TAPPI, Acid-insoluble lignin in wood and pulp, modified method based on Test Method T-222 om-88, 1988; TAPPI, Acid-soluble lignin in wood and pulp, Useful Method UM-250, 1991).[28] The water washed *T. pungens* grass sample comprised 33 % (w/w) cellulose, 44 % (w/w) hemicellulose, and 23 % (w/w) lignin. In comparison, after delignification and bleaching steps, the amounts of cellulose, hemicellulose and lignin were found to be 55 %, 42 %, and 3 % (w/w), respectively.

Fibrillation using a high pressure homogenizer

A 0.3 % (w/v) dispersion of bleached pulp of *T. pungens* with an average diameter of 12 ± 1.4 µm was passed between one and 15 times through a high pressure homogenizer (EmulsiFlex-C5 Homogenizer, Avestin Inc, Ottawa, Canada) at three different applied pressures of 35, 100, and 150 MPa. For comparison, the effect of homogenization on purified cellulose, a 0.3 % (w/v) dispersion of MCC with a diameter in the range of 10 – 20 µm and length in the range of 38 – 60 µm, was passed one time through the homogenizer at 150 MPa.

Preparation of cellulose nanopaper

Thin paper from the NFC dispersion was produced via the vacuum filtration method using a Büchner funnel fitted with a cellulose acetate membrane filter (pore size: 0.45 µm, diameter: 47 mm. Advantec, Toyo Roshi Kaisha, Ltd, Japan). Prior to filtration, 20 mL of 0.3 % (w/v) dispersion was diluted with 20 mL water and stirred for 24 hours, and then filtration was continued until the wet sheet of NFC was formed. The wet sheet was peeled from the filter paper, placed between Teflon sheets and compression-moulded at 103 °C using a hydraulic press with (a) no significant pressure, and (b) 1000 psi for one hour, in order to obtain nanopaper samples with high and low porosities, respectively. The nanopaper samples were further conditioned at room temperature and 65 % relative humidity for a week prior to testing. (Figure S1).
The density of NFC nanopaper was calculated by measuring the weight of paper and dividing it by its volume. Nanopaper thickness was measured using a micrometer and the corresponding porosity was estimated using the following equation (1):

$$\text{Porosity} = 1 - (\rho_{\text{NFCpaper}}/\rho_{\text{cellulose}}) \quad (1)$$

where $\boldsymbol{\rho}_{\text{nanopaper}}$ and $\boldsymbol{\rho}_{\text{cellulose}}$ represent the density of obtained NFC film and neat cellulose (1460 kg/m^3), respectively.[29]

Characterization

Scanning electron microscopy (SEM): In order to view the morphology of native fibres, the water-washed and air-dried grass fibers were used. Prior to scanning, fibre samples were further dried under vacuum overnight at 50 °. These dried samples were mounted on sticky carbon tape on the SEM stubs and then gold coated using a SPI-Module sputter coater (SPI supplies, Pensylvania, U.S.A). Samples were imaged using a Neoscope JCM-5000 (JEOL, Tokyo, Japan) operating at 10 kV.
Transmission electron microscopy (TEM): A 0.04 mg/mL dispersion of nanocellulose in water was sonicated at 25 % amplitude for five minutes (using Q500 Sonicator). 1µL of dispersion was spotted onto Formvar coated 200 mesh copper/palladium grid (ProSciTech, Queensland, Australia) and

allowed to dry at room temperature. The sample was then stained with a 2 % (v/v) uranyl acetate (UA) aqueous solution for ten minutes in the absence of light. After removing excess UA with a paper tip, the grid was allowed to dry at room temperature. Finally the grid was examined on a JEOL 1011 TEM (JEOL Pty Ltd., Frenchs Forest, Australia) at 100 KV and images were captured on a SIS Morada 4K CCD camera system. The average diameter of nanofibrils was measured using digital image analysis (Image J). For each sample, the diameter of nanofibrils was measured from 102 randomly selected nanofibers in several TEM images with the same magnification. Measuring the length of long and rope-like NFC was achieved using cryo-TEM and AutoCAD, as explained in the supplementary A and B information.

Attenuated total reflectance (ATR) Fourier transform infrared spectroscopy (FTIR). Fourier transform infrared (FTIR) spectroscopy was performed on a Thermo-Nicolet 5700 ATR FTIR spectrometer equipped with a Nicolet Smart Orbit single bounce, diamond ATR accessory (thermos-electron Crop., Waltham, USA). Freeze dried fibre samples obtained from each stage of modifications were directly pressed onto the diamond internal reflection element of the ATR accessory. Spectra were recorded in the wave number range of 4000 to 500 cm^{-1} and at a resolution of 4 cm^{-1} from 128 scans.

X-Ray diffraction. X-Ray diffraction analysis of the water-washed, air-dried and ground grass fibre samples and also freeze-dried fibre/ nanofibre samples following delignification, bleaching and homogenisation processes, respectively, was conducted on a Bruker D8 Advance X-ray diffractometer (Bruker, Karlsruhe, Germany) with a 0.2 mm slit. Graphite-filtered Cu-Ka radiation was generated at 30 kV and 20 mA. Samples were put in the sample holder and scanned over a range of 2θ = 5°- 40° with a speed of 1°/min. Crystallinity index which expresses the relative degree of crystallinity was measured using equation (2):[30]

$$\mathrm{CrI} = ((\mathrm{I}_{002} - \mathrm{I}_{\mathrm{am}})/\mathrm{I}_{002}) \times 100 \quad (2)$$

Where I_{002} represents the intensity of the both amorphous and crystalline regions and I_{am} is the intensity of amorphous parts in XRD spectra.

The mean size of crystalline regions, which is another parameter to evaluate the effect of different treatments on the crystalline structure of nanocellulose samples, was calculated using Debye-Scherrer equation (3):[31-33]

$$D = \kappa\lambda/\beta\cos\theta \quad (3)$$

Where K is the shape factor and is approximately = 0.89, β is the line width in radians at half the maximum intensity of I_{200} , λ is the wave length of the radiation (0.154 nm) and θ is the scattering angle of the peak (200).

Mechanical properties: The tensile properties of the two porous NFC nanopaper samples were measured at room temperature using an Instron model 5543 universal testing machine (Instron Pty Ltd., Melbourne, Australia) fitted with a 500 N load cell. A total of five rectangular strips of each sample, having dimensions of 25 mm in length and 6 mm in width, were tested at a cross-head speed of 1mm/min and a gauge length of 10 mm.

Transverse elastic modulus: 0.04 mg/ml of NFC dispersion in water was dried on a freshly cleaved mica surface and imaged using AFM. All the AFM measurements were obtained using a Cypher S AFM (Asylum Research/Oxford Instruments, Santa Barbara, CA). The cantilevers used were Tap 300 (Budget Sensors, Bulgaria) with a nominal resonance frequency of 300 kHz and a nominal spring constant of 40 N/m. The elastic modulus of individual cellulose nanofibrils was measured by AM-FM (Amplitude Modulation-Frequency Modulation). AM-FM works based on simultaneous monitoring of two distinct normal modes of vibration of the cantilever. Briefly, the topographic feedback operates in normal tapping mode, providing non-invasive, high quality imaging. The second mode drive frequency is adjusted to keep the phase at 90 °, on resonance. This resonant frequency is a sensitive measure of the tip-sample interaction. After the cantilever was calibrated using Ultra High Molecular Weight Polyethylene having a Young's Modulus of 1.26 GPa, the tip was retracted and the calibrated sample was replaced by the sample of interest.[34, 35]

Results and discussion

Plant traits of *T. Pungens*

The composition of lignocellulosic components in *Triodia pungens* water washed grass and bleached pulp showed that prior to delignification and bleaching the grass had a hemicellulose content of 44 % (w/w) and this reduced to 42 % following delignification and bleaching (note these percentages are with respect to the total lignocellulosic mass of the material). Interestingly, the hemicellulose content did not decrease significantly after delignification or bleaching of the water washed grass, demonstrating that the high hemicellulose content of the grass is maintained through to the final nanocellulose product. No doubt the very mild delignification and bleaching conditions used in our method is a contributing factor. We postulate that the high amount of hemicellulose in *T. pungens* grass is associated with a strategy of the plant to help it retain water during periods of drought (hemicellulose is mainly responsible for moisture absorption and retention in the plant fibre). Fortuitously, during spinifex NFC processing this hemicellulose is plasticized by absorbing moisture and consequently results in a decrease in the cohesion forces between the cellulose fibrils, making cell wall delamination easier[36, 37], avoiding blocking of the constriction chamber of the homogenizer, and thereby decreasing the required overall energy consumption. In order to better understand this, the spinifex leaf morphology was characterised by SEM as shown in Figure 1. *Triodia* species have hard leaves with a C_4 leaf anatomy which are reinforced with sclerenchyma and thick-walled parenchyma. [27, 38] Chlorophyll-rich bundle sheaths are arranged around the stomatal groves and positioned between vascular bundles. The SEM images of leaf transverse sections

show dense sclerenchyma and parenchyma cells with pit apertures (Figure 1). Cellulose microfibrils are organized in a looser network embedded in an abundant matrix consisting of hemicelluloses, rather than a tight lignin network. [39, 40] We hypothesise that as a result of this loose and arguably weaker microfibrillar interaction with the matrix, micro and nanofibrils can more easily be separated from one another.

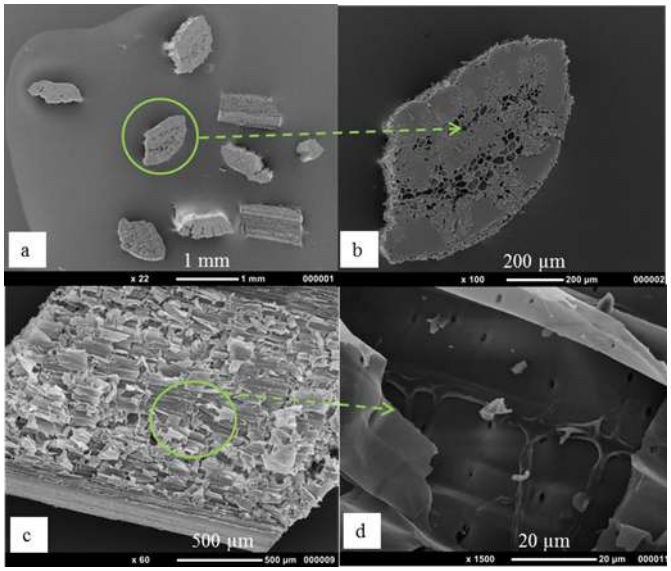

Figure 1. SEM micrographs of water-washed and air-dried *Triodia pungens* grass; a) and b) transverse sections of grass at low magnification (scale bar: 1 mm) and higher magnification (scale bare: 200 µm), c) and d) longitudinal sections of grass showing parenchyma cells at low magnification (scale bar 500 µm) and parenchyma cells with pit apertures at higher magnification (scale bar 20 µm)

Pulping of *T. Pungens*

Prior to fibrillation, pulp of *T. Pungens* was prepared by delignification with alkaline solution at low concentration (~2 %) and bleached with sodium chlorite solution (~1 %, 2 times). FTIR spectral analysis was used to follow the functional group changes in the fibers. FTIR spectra (See Figure S2 in Supplementary Information) show characteristic peaks in the region of 950 - 1200 cm^{-1} for the C-O-C pyranose ring and a band at 896 cm^{-1} for the glycosidic –C-H groups with a ring contribution indicating the β-glycosidic linkage between anhydroglucoses cellulose.[41-43] A decrease in the peak with a maximum occurring at around 2900 cm^{-1} (responsible for C-H stretching) indicates the removal of hydrophobic lignin and other waxy components after delignification and bleaching. The peak at 1734 cm^{-1} (C=O stretching) is attributed to the vibration of the acetyl and uronic ester groups, from hemicellulose or ester bonds of the carboxylic groups of ferulic and p-coumaric acids of lignin or/and hemicellulose[44] showed a decrease in the intensity after delignification and bleaching that can be attributed to the breakage of the ester linkages of carboxylic groups of lignin and/or hemicellulose and oxidation of the terminal glucopyranose unit.[45] Another possibility is that carboxyl or aldehyde absorption could be arising from the opened terminal glycopyranose rings or oxidation of the C-OH groups.[46] The other band around 1240 cm^{-1}, which corresponds to the axial asymmetric strain of =C-O- in ether, ester, and phenol groups of lignin, also decreases in the bleached fibres.

Nanofibrillation of *T. Pungens*

Nanofibrillation was performed via homogenization of the aqueous suspension of bleached pulp by systematically varying the pressure and number of passes to optimize the process. It was found that high pressure homogenization has a noticeable effect on reducing the diameter of fibres, and producing long, thin nanofibrils with a complex and web-like structure. A stable and homogeneous (white coloured) dispersion of NFC in water was obtained after homogenization (Figure S3). The diameters of the nanofibres were measured from TEM images of the suspensions obtained after homogenisation under different number of passes and pressures (Table 1). It can be seen that the NFCs resulting from homogenisation under different conditions exhibited almost the same nanofibre diameter (with an average of 3.5 nm). For example, homogenization of a 0.3 % (w/v) bleached pulp at 35 MPa and only after one pass, yielded NFC with an average diameter of 3.7 ± 1 nm (Figure 2) as measured from this type of image).

Table 1. The average diameter of nanofibrils (nm) produced by homogenization as a function of increasing numbers of passes and applied pressures

Pressure	1 pass	5 passes	10 passes	15 passes
150 MPa	3.5 ± 0.8	3.2 ± 0.7	3.3 ± 0.8	3.2 ± 0.8
100 MPa	3.5 ± 0.6	-	-	-
35 MPa	3.7 ± 1.0	-	-	-

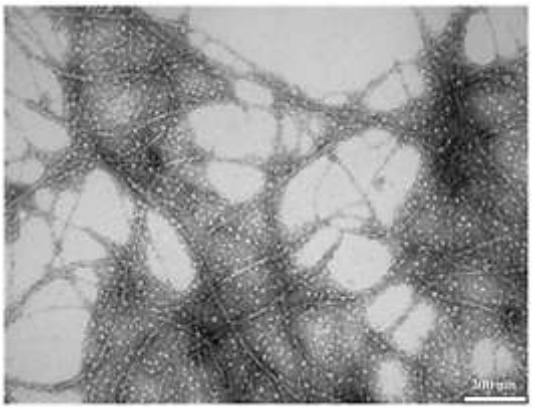

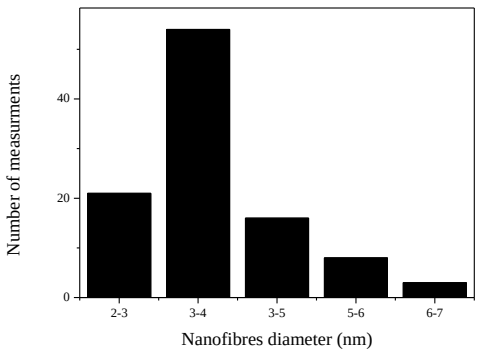

Figure 2. a) TEM image and b) histogram of average diameter of NFC from *T. pungens* obtained after one single pass at 35 MPa

The length-to-thickness ratio of *T.pungens* nanofibrils is also very high,[10-12, 47] however this high aspect ratio primarily results from the small diameter of nanofibrils (1-8 nm).

It is not easy to measure the length of the individual NFC on the TEM images (Figure 2), as nanofibrils are contorted and entangled with each other with a random in-plane orientation so the start and end points of nanofibrils are not always clear or possible to find. Also, as the NFC is dispersed in water, the strong secondary inter-fibril interactions such as hydrogen bonding will increase upon drying, and this makes the characterization of these long, ropey NFC quite different from the rod-like materials such as CNC and tunicate whiskers .[48] So the length of thicker bundles of nanofibrils which have an average diameter of 10 nm was measured in the lower magnification TEM images (as it can be seen in Figure 3a) with Auto CAD (Supplementary Information A) to enable observation of the whole long bundle in a single image, while the length of individual nanofibrils with an average diameter of about 3.5 nm was measured with cryo-TEM (the movie provided in the Supplementary Information B shows three dimensional images of NFC which were taken by cryo-TEM. The length of individual nanofibrils was measured using this approach). The average aspect ratio of a bundle of a few nanofibrils produced from homogenization of a 0.3 % (w/v) fibre dispersion for only one pass at 150 MPa pressure, with an average diameter of 10.7 ± 3.9 nm and an average length of 5773 ± 1700 nm, is 540 ± 166, and ranging from 305 to 727. The average aspect ratio of individual fibrils of the same sample with an average diameter of 3.5 ± 0.8 nm and an average length of 1686 ± 591 nm, is 527 ± 185, and ranging from 266 and 958.

Here we must emphasise that fibrillation with one pass was performed without any further chemical and enzymatic pretreatments on bleached pulp. Such pretreatments are necessary in the majority of contemporary protocols for obtaining NFC from wood or plant pulps.

Nanofibrillation via high-pressure homogenization at low energy

The NFC obtained by homogenization was further compared with the more common and commercially available pure cellulose, MCC. Figure 3 compares the TEM image of the *T. pungens* NFC with the nanocrystals obtained via homogenization of an aqueous suspension of MCC at a pressure of 150 MPa for one pass. Homogenization of MCC resulted in a significant reduction in its particle size and produced regular rod shaped cellulose nanocrystals with an average diameter of 5.6 ± 1.4 nm and an average length of 216 ± 70 nm. It can be seen that although the diameter of MCC nanocrystals and *T. pungens* NFC are almost identical, the length of *T. pungens* nanofibrils is still significantly higher than the MCC nanocrystal. A significant finding from this study is the ease of fibrillating *T. pungens* bleached pulp into nanoscale fibrils after just one pass, even with the low pressure setting, and without encountering clogging issues.

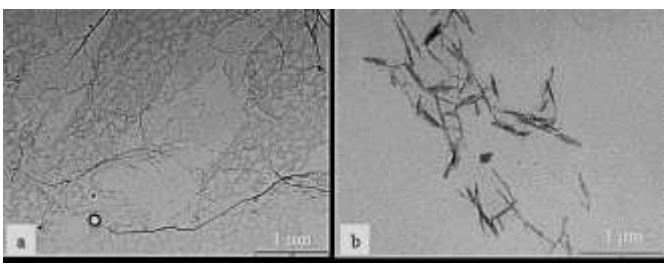

Figure 3. TEM micrograph of; a) *T. pungens* NFC after homogenisation at 35 MPa pressure, and b) cellulose nanocrystals obtained from commercial microcrystalline cellulose. Both images were obtained via homogenization at 150 MPa after one pass

This contrasts with other comparable published studies which found that a minimum of three passes was necessary for NFC preparation, often in combination with additional treatment with acid, alkali or polyelectrolyte in order to reduce the number of passes (Table 2). From a technological standpoint, the ease-of-fibrillation of *T. pungens* pulp is crucial in terms of minimising the energy consumption by reducing the number of passes and applied pressure, and also the associated cost of the process.[49-52] It is known that the fibrillation of pulp into microfibrillated cellulose is facilitated by the presence of hemicellulose, which is most likely due to the negative charges on hemicellulose that lead to charge repulsion between the fibrils.[36] Additionally we believe that this high water-swellable hemicellulose content "toughens" the NFC, rendering them more fracture-resistant during the conditions of high shear, turbulence and cavitation imposed during homogenization. Table 2 compares the chemical composition of bleached pulp of

different plant feedstocks and using different processing routes, as reported in the scientific literature. Significantly, it can be seen that the amount of hemicellulose remaining in the bleached pulp of *T. pungens* is higher than that reported for other sources of cellulose.

RSC Advances

RSCPublishing

PAPER

Table 2. Comparison chemical composition of the bleached pulp obtained from different sources and treatments of cellulose

Source of cellulose	Mechanical treatment	Diameter (nm) of fibrils	Length (μm) of fibrils	Cellulose (%)	Hemicellulose (%)	Lignin (%)	Ref
Bleached *T. pungens* pulp	Homogenization for 1 pass at 150 MPa	1-8	1-7	55	42	3	
Bamboo fibre	Ultrasonication for 30 min at 1200 W and centrifugation to separate thicker fibrils	30-80	Up to 10	93.3	6.7	0.1	9
Sugar-beet pulp	Ultrasonication at 20 kHz and 500 W for 4 min followed by heating to 65 °C for 20 min then homogenization for 10 passes at 30 and 38 to 40 MPa	2-15	-	80.33	6.9	-	53
Sugar beet pulp	Homogenization for 1 pass at 20 MPa then 10 passes at 80 MPa	20-70	0.2-1	82.83	7.01	0	54
Abaca	Homogenization for 5-7 passes at 30 MPa followed by 10 passes at 60 MPa	20	Several microns	86.84	13.5	-	55
Hemp	Homogenization for 5-7 passes at 30 MPa followed by 10 passes at 60 MPa	30-50	5	91.50	8.51	-	55
Bleached eucalyptus fibre	Ultrasonication for 30 min followed by homogenization for 40 passes at 100 MPa	1000-5000	Few micron	80.35	13.52	0.20	56
Softwood bleached kraft pulp	Double-cylinder homogenizer at 10000 rpm for 2 min followed by ultrasonic homogenizer at 19.5 kHz and 300 W for 2 min then centrifugation to separate thicker fibrils	3-4	0.2-2.5	90	10	-	57
Bleached eucalyptus pulp	Disc refiner several passes followed by ultrasonication for 7h at 50% amplitude and 80W, then centrifugation to separate thicker fibrils	20-50	-	85.2	13.9	0.1	58
Empty Palm Fruit Bunch Fibers	HCl and $NaHCO_3$ treatment followed by PFI mill, then microflouidization for 5 passes at 55 MPa	-	AR= 90-110	75.8	6.2	9	59
Wheat straw	Cryocrushing followed by homogenization for 20 passes at 30 MPa	10-80	Few microns	84.6	6	9.4	60
Holocellulose pulp	Masuko grinder for 1 pass at 1500 rpm	10-20	-	77.7	21.4	0.1	37

*AR is aspect ratio calculated by length/diameter of fibres

RSC Advances RSCPublishing

PAPER

Crystallinity of *T.pungens* NFC

Cellulose fibres are comprised of crystalline and amorphous regions. The degree of crystallinity cannot be exactly defined, as the crystalline portions are neither perfect crystals, nor are the non-crystalline portions completely disordered.[46] It is also known that the crystallinity of cellulose can be affected dramatically by different calculation methods because of the overlapping and broadened diffraction peaks of cellulose. [32] So the most widely used method for measuring the crystallinity of plant fibre was applied based on Segal et al. [30] method for all *T. pungens* samples. Figure 4 compares the XRD patterns of the obtained nanofibrils with untreated, delignified and bleached fibres. The observed XRD peaks around 2θ = 16 (broad peak comprising 101 and 10$\bar{1}$ planes), 22.6 (002 plane) and 35 are representative of a typical polymorph of cellulose I. The broadening of the peak at around 16 for all sample may indicate the presence of hemicellulosic components such as xylan.[61]

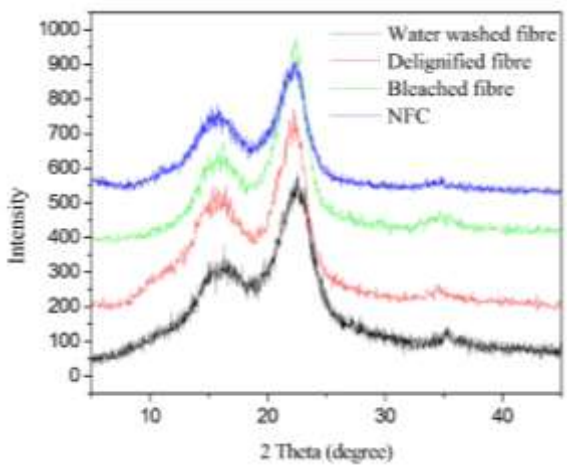

Figure 4. X-Ray diffraction patterns for water washed, delignified, bleached fibres and NFC of *T. pungens*

The similarity of the patterns indicate that the cellulose I polymorph was not disrupted by the mild conditions applied. The crystallinity index (CrI) of *T. Pungens* fibre was increased after delignification (71 %) and bleaching (74 %) from its native crystallinity (59 %) indicating the removal of non-cellulosic components[62] (See Table S1 in Supplementary Information). After homogenization, the CrI of NFC slightly decreased (to 69 %) which may be due to damage or disordering of the nanocrystalline domains in the nanofibers upon the application of mechanical energy. The similar trend was observed in crystalline domain size. The thickness of crystalline domains is slightly increased after delignification, bleaching and homogenization processes.

Mechanical properties of nanopaper

Figure 5 and table 3 compare the stress-strain curves and mechanical property profiles for nanopapers obtained by vacuum filtration and different compression (negligible versus 1000 psi) from the suspension of *T. Pungens* NFC (0.15 w/v %) concentration. The nanopaper formed using higher compression (~ 89 μm thickness) obtained from *T. Pungens* NFC with a porosity of 22 %, showed 3.2 GPa Young's modulus, 18 %, tensile strain, 84 MPa tensile stress, and 12 MJm^{-3} toughness (work at fracture). The better mechanical properties for the nanopaper with lower porosity may be due to the existence of "compacted" hemicellulose which changed the interfibrillar interactions after compression molding at a temperature of 103 °C.

Table 3: Tensile properties of nanopapers made from the NFC suspension of *T. Pungens*

Porosity (%)	Young's Modulus (GPa)	Tensile Strain at Break (%)	Tensile Stress (MPa)	Work at Fracture (MJm^{-3})
22	3.2 ± 0.2	18 ± 0.2	84 ± 5	12.3 ± 2
32	3 ± 0.1	12 ± 0.3	67 ± 0.1	6 ± 0.2

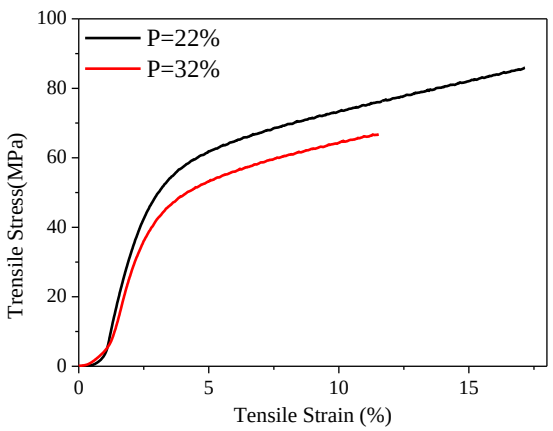

Figure 5. Tensile curves of thin papers with different porosities (P) prepared from the NFC suspension (0.15 w/v %) of *T. pungens*

These favourable properties are due to the high aspect ratio nanofibril orientation and network structure. It can be seen that the overall toughness of *T. pungens* derived NFC (area under the tensile curve) is very high, as corroborated in Table S2 in

comparison with other reported values for nanofibers. Clearly the mechanism at play is very complex, however this could be associated with interfibril debonding, bending and plasticity of nanofibrils, slippage of high aspect ratio and well-entangled nanofibrils, and ultimately, high tensile strength of individual nanofibrils enabling quite a high plastic deformation before breakage.[48]

Despite a relatively high porosity, the nanopaper samples obtained from *T. pungens* NFC strained to a larger value in comparison with the other sources of cellulose (Table S2). [29, 63, 64] This could be due to the smaller and more homogeneously distributed voids, reasonably strong interfibril adhesion, and the strength of individual nanofibrils.[48] As already mentioned, one very important differentiating factor for *T. pungens* NFC is the unusually-high hemicellulose content and the flexibility and toughness [37] that this imparts to nanofibrils through strong but "forgiving" and labile interfibre bonding, which reportedly is beneficial for imparting toughness and flexibility to NFC nanopaper.[37, 65, 66]

Elastic modulus of single nanofibrils

In order to gain a better understanding of the mechanical properties of individual fibrils of *T. pungens* NFC, particularly with respect to polymer nanocomposite applications, the transverse elastic modulus of individual nanofibrils was estimated using AFM. In all reported methods,[67-70] the force-displacement curves were acquired by AFM then fitted by several different models to estimate the transverse elastic modulus. In this study the AM-FM (Amplitude Modulation-Frequency Modulation) method was employed. This relatively new approach was applied to measure the transverse elastic modulus of a single nanofibril. The AFM images and modulus profiles in Figure 6 show the elastic modulus of *T. pungens* NFC with an average diameter of 3.5 ± 0.8 nm.

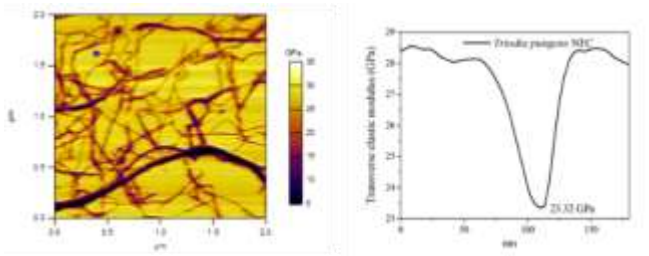

Figure 6. Transverse elastic modulus of a single *T. pungens* nanofibril as determined by AM-FM

It was determined that the elastic modulus of *T. pungens* NFC is in the range of 19 - 24 GPa. The elastic modulus range of *T. pungens* NFC is a little lower than most reported values for CNCs, which is consistent with our findings that our NFC has a relatively high amorphous hemicellulose content, giving them more toughness and flexibility, rather than stiffness, as expected for CNCs (we could not find any other published values for the transverse elastic modulus of other NFC or MFC variants). For comparison, the transverse elastic modulus for wood-derived CNC has been reported at about 18 - 50 GPa,[67] 24.8 and 17.7 GPa for wood and cotton-derived CNCs, respectively ,[68] and 2 - 25 GPa for tunicate CNC.[69, 70] These elastic modulus indicate strong inter and intramolecular hydrogen bonding in spinifex NFC. These results could also be explained by the higher crystallinity and lower number of defects in our NFC crystal structure.[68]

Conclusion

High aspect ratio nanofibrils were obtained through the high pressure homogenization of delignified and bleached *Triodia pungens* semi-arid grass fibres. The fibrillation of pretreated fibres produces very high aspect ratio NFC, even after only one pass through the homogenizer, and without any clogging issues, indicating that long nanofibrils with a very small diameter can be obtained by very mild pulping and significantly lower energy consumption. Applying different pressure, and also varying the number of passes through the homogenizer produced almost the same result in terms of nanofibril diameter and length. An unusually high remnant hemicellulose content of approximately 42 % appears to be an important factor in this more amenable fibrillation trait, apparently acting to "toughen" the NFC, rendering them more fracture-resistant during the conditions of high shear, turbulence and cavitation imposed during homogenization. Despite this, the NFC obtained from *T. pungens* had a relatively high crystallinity of about 69 %, and the transverse elastic modulus of a single nanofibril was measured to be in the range of 19 - 24 GPa, slightly lower than most credible reports for CNC transverse elastic modulus. Not surprisingly, the nanopaper with low porosity produced from high aspect ratio NFC showed a high work at fracture, which indicates a high toughness; a trait that could, for example, prove to have utility in nonwoven membrane, packaging and polymer composite applications. A broader social significance of our finding is the potential that commercial harvesting and extraction of spinifex nanofibres could provide for the foundation of new enterprises for remote Australian Aboriginal groups currently suffering economic poverty.

Acknowledgments

The authors gratefully acknowledge the financial support from Australian Research Council (under ARC Discovery Grant No. DP0877161). They also acknowledge the Aboriginal collaborator, Dugalunji Aboriginal Corporation in Camooweal for project collaboration and the supply of grass samples, Dr Harshi Gamage for her helpful discussion about the morphology of spinifex grass and Prof Robert Moon and Mr Ryan Wagner at Purdue University for their helpful discussions for AM-FM analysis. The authors acknowledge the facilities, and the scientific and technical assistance, of the Australian Microscopy & Microanalysis Research Facility at the Centre

for Microscopy and Microanalysis, The University of Queensland and Dr Isabel Marrow and Dr Gary Morgan for taking images. The AM-FM analysis was performed in part at the Queensland node of the Australian National Fabrication Facility, a company established under the National Collaborative Research Infrastructure Strategy to provide nano and micro-fabrication facilities for Australia's researchers.

Notes and References

1. R. J. Moon, A. Martini, J. Nairn, J. Simonsen and J. Youngblood, *Chemical Society Reviews*, 2011, **40**, 3941-3994.
2. X. M. Dong, T. Kimura, J.-F. Revol and D. G. Gray, *Langmuir*, 1996, **12**, 2076-2082.
3. J. Mendez, P. K. Annamalai, S. J. Eichhorn, R. Rusli, S. J. Rowan, E. J. Foster and C. Weder, *Macromolecules*, 2011, **44**, 6827-6835.
4. P. K. Annamalai, K. L. Dagnon, S. Monemian, E. J. Foster, S. J. Rowan and C. Weder, *ACS Applied Materials & Interfaces*, 2013, **6**, 967-976.
5. K. Spence, R. Venditti, O. Rojas, Y. Habibi and J. Pawlak, *Cellulose*, 2011, **18**, 1097-1111.
6. Q. Li and S. Renneckar, *Cellulose*, 2009, **16**, 1025-1032.
7. K. L. Spence, R. A. Venditti, O. J. Rojas, Y. Habibi and J. J. Pawlak, *Cellulose*, 2011, **18**, 1097-1111.
8. I. Siró and D. Plackett, *Cellulose*, 2010, **17**, 459-494.
9. W. Chen, H. Yu and Y. Liu, *Carbohydrate Polymers*, 2011, **86**, 453-461.
10. T. Saito, Y. Nishiyama, J.-L. Putaux, M. Vignon and A. Isogai, *Biomacromolecules*, 2006, **7**, 1687-1691.
11. T. Saito, S. Kimura, Y. Nishiyama and A. Isogai, *Biomacromolecules*, 2007, **8**, 2485-2491.
12. L. Wagberg, G. Decher, M. Norgren, T. Lindstrom, M. Ankerfors and K. Axnas, *Langmuir*, 2008, **24**, 784-795.
13. C. Aulin, J. Netrval, L. Wagberg and T. Lindstrom, *Soft Matter*, 2010, **6**, 3298-3305.
14. N. Lavoine, I. Desloges, A. Dufresne and J. Bras, *Carbohydrate Polymers*, 2012, **90**, 735-764.
15. W. Stelte and A. R. Sanadi, *Industrial & Engineering Chemistry Research*, 2009, **48**, 11211-11219.
16. H. Charreau, M. L. Foresti and A. Vazquez, *Recent patents on nanotechnology*, 2013, **7**, 56-80.
17. K. Missoum, M. N. Belgacem and J. Bras, *Materials*, 2013, **6**, 1745-1766.
18. *Australia Pat.*, PCT/AU2014/050368, 2013.
19. B. Rice and M. Westoby, *Australian Journal of Ecology*, 1999, **24**, 563-572.
20. G. E. Allan, Southgate, R., in *Flammable Australia: The fire regimes and biodiversity of a continent*, eds. R. Bradstock, J. Williams and M. Gill, Cambridge, 2002, pp. 145–176.
21. M. Lazarides, *Australian Systematic Botany*, 1997, **10**, 381–489.
22. J. R. McWilliam and K. Mison, *Australian Journal of Plant Physiology* 1974, 171–175.
23. S. W. L. Jacobs, ed. E. HCogger, Australian Museum: Sydney, 1984, pp. 131–142.
24. S. W. L. Jacobs, Systematic position of the genera Triodia R. Br. and Plectrachne Henr. (Gramineae), NSW, 1971.
25. S. W. L. Jacobs, in *Desertified Grasslands:Their Biology and Management*, ed. G. P. Chapman, Academic Press, London, 1992, pp. 47–62.
26. S. Craig and D. Goodchild, *Australian Journal of Botany*, 1977, **25**, 277-290.
27. H. K. Gamage, S. Mondal, L. A. Wallis, P. Memmott, D. Martin, B. R. Wright and S. Schmidt, *Australian Journal of Botany*, 2012, **60**, 114-127.
28. R. C. Pettersen and V. H. Schwandt, *Journal of wood chemistry and technology*, 1991, **11**, 495-501.
29. H. Sehaqui, Q. Zhou, O. Ikkala and L. A. Berglund, *Biomacromolecules*, 2011, **12**, 3638-3644.
30. L. Segal, J. J. Creely, A. E. Martin and C. M. Conrad, *Textile Research Journal*, 1959, **29**, 786-794.
31. R. Avolio, I. Bonadies, D. Capitani, M. E. Errico, G. Gentile and M. Avella, *Carbohydrate Polymers*, 2012, **87**, 265-273.
32. A. Thygesen, J. Oddershede, H. Lilholt, A. B. Thomsen and K. Ståhl, *Cellulose*, 2005, **12**, 563-576.
33. P. Scherrer, *Nachr. Ges. Wiss*, 1918, 98-100.
34. G. Lamour, C. K. Yip, H. Li and J. Gsponer, *ACS Nano*, 2014, **8**, 3851-3861.
35. S. Bertolazzi, J. Brivio, A. Radenovic, A. Kis, H. Wilson, L. Prisbrey, E. Minot, A. Tselev, M. Philips, M. Viani, D. Walters and R. Proksch, *MicroscopyandAnalysis*, 2013, **27**, 21-24 (AM).
36. S. Arola, J.-M. Malho, P. Laaksonen, M. Lille and M. B. Linder, *Soft Matter*, 2013, **9**, 1319-1326.
37. S. Iwamoto, K. Abe and H. Yano, *Biomacromolecules*, 2008, **9**, 1022-1026.
38. J. R. McWilliam and K. Mison, *Australian journal of plant physiology*, 1974, **1**, 5.
39. Y. Habibi, M. Mahrouz and M. R. Vignon, *Food Chem*, 2009, **115**, 423-429.
40. E. Dinand, H. Chanzy and M. R. Vignon, *Food Hydrocolloid*, 1999, **13**, 275-283.
41. B. Xiao, X. F. Sun and R. Sun, *Polymer Degradation and Stability*, 2001, **74**, 307-319.
42. R. Zuluaga, J. L. Putaux, J. Cruz, J. Vélez, I. Mondragon and P. Gañán, *Carbohydrate Polymers*, 2009, **76**, 51-59.
43. S. Elanthikkal, U. Gopalakrishnapanicker, S. Varghese and J. T. Guthrie, *Carbohydrate Polymers*, 2010, **80**, 852-859.
44. X. F. Sun, F. Xu, R. C. Sun, P. Fowler and M. S. Baird, *Carbohydrate Research*, 2005, **340**, 97-106.
45. R. M. Sheltami, I. Abdullah, I. Ahmad, A. Dufresne and H. Kargarzadeh, *Carbohydrate Polymers*, 2012, **88**, 772-779.
46. E. Abraham, B. Deepa, L. A. Pothan, M. Jacob, S. Thomas, U. Cvelbar and R. Anandjiwala, *Carbohydrate Polymers*, 2011, **86**, 1468-1475.
47. M. Paakko, M. Ankerfors, H. Kosonen, A. Nykanen, S. Ahola, M. Osterberg, J. Ruokolainen, J. Laine, P. T. Larsson, O. Ikkala and T. Lindstrom, *Biomacromolecules*, 2007, **8**, 1934-1941.
48. M. Henriksson, L. A. Berglund, P. Isaksson, T. Lindström and T. Nishino, *Biomacromolecules*, 2008, **9**, 1579-1585.

49. M. Österberg, J. Vartiainen, J. Lucenius, U. Hippi, J. Seppälä, R. Serimaa and J. Laine, *ACS Applied Materials & Interfaces*, 2013, **5**, 4640-4647.
50. Swerin, *Nordic Pulp & Paper Research Journal*, 1990, **05**, 188-196.
51. K. Junka, I. Filpponen, L.-S. Johansson, E. Kontturi, O. J. Rojas and J. Laine, *Carbohydrate Polymers*.
52. G. Chinga-Carrasco, N. Kuznetsova, M. Garaeva, I. Leirset, G. Galiullina, A. Kostochko and K. Syverud, *J Nanopart Res*, 2012, **14**, 1-10.
53. G. Agoda-Tandjawa, S. Durand, S. Berot, C. Blassel, C. Gaillard, C. Garnier and J. L. Doublier, *Carbohydrate Polymers*, 2010, **80**, 677-686.
54. M. Li, L.-j. Wang, D. Li, Y.-L. Cheng and B. Adhikari, *Carbohydrate Polymers*, 2014, **102**, 136-143.
55. S. Alila, I. Besbes, M. R. Vilar, P. Mutjé and S. Boufi, *Industrial Crops and Products*, 2013, **41**, 250-259.
56. I. Urruzola, L. Serrano, R. Llano-Ponte, M. Ángeles de Andrés and J. Labidi, *Chemical Engineering Journal*, 2013, **229**, 42-49.
57. T. Isogai, T. Saito and A. Isogai, *Cellulose*, 2011, **18**, 421-431.
58. G. H. D. Tonoli, E. M. Teixeira, A. C. Correa, J. M. Marconcini, L. A. Caixeta, M. A. Pereira-da-Silva and L. H. C. Mattoso, *Carbohydrate Polymers*, 2012, **89**, 80-88.
59. A. Ferrer, I. Filpponen, A. Rodriguez, J. Laine and O. J. Rojas, *Bioresource Technol*, 2012, **125**, 249-255.
60. A. Alemdar and M. Sain, *Composites Science and Technology*, 2008, **68**, 557-565.
61. Noor Afizah Rosli, Ishak Ahmad and I. Abdullah., *Bioresources*, 2013, **8**, 1893-1908.
62. W. Chen, H. Yu, Y. Liu, P. Chen, M. Zhang and Y. Hai, *Carbohydrate Polymers*, 2011, **83**, 1804-1811.
63. M. Osterberg, J. Vartiainen, J. Lucenius, U. Hippi, J. Seppala, R. Serimaa and J. Laine, *ACS Applied Materials & Interfaces*, 2013, **5**, 4640-4647.
64. M. Jonoobi, A. P. Mathew and K. Oksman, *Industrial Crops and Products*, 2012, **40**, 232-238.
65. L. Li, S. Lee, H. L. Lee and H. J. Youn, *Bioresources*, 2011, **6**, 721-736.
66. *US Pat.*, 20040200587 2004.
67. R. R. Lahiji, X. Xu, R. Reifenberger, A. Raman, A. Rudie and R. J. Moon, *Langmuir*, 2010, **26**, 4480-4488.
68. A. Pakzad, J. Simonsen, P. A. Heiden and R. S. Yassar, *Journal of Materials Research*, 2012, **27**, 528-536.
69. X. W. Wu, R. J. Moon and A. Martini, *Cellulose*, 2013, **20**, 43-55.
70. R. Wagner, R. Moon, J. Pratt, G. Shaw and A. Raman, *Nanotechnology*, 2011, **22**.

Footnote

Electronic Supplementary Information (ESI) available. See DOI:

RSC Advances

RSCPublishing

PAPER